Journal of Power Sources 270 (2014) 262–272

Contents lists available at ScienceDirect

Journal of Power Sources

journal homepage: www.elsevier.com/locate/jpowsour

A support vector machine-based state-of-health estimation method for lithium-ion batteries under electric vehicle operation

Verena Klass*, Mårten Behm, Göran Lindbergh

Applied Electrochemistry, Department of Chemical Engineering and Technology, KTH Royal Institute of Technology, Teknikringen 42, SE-100 44 Stockholm, Sweden

HIGHLIGHTS

- We present a novel SOH estimation method based on on-board available battery data.
- Standard performance tests are applied virtually to a data-driven battery model.
- The method conveniently yields the same figures of merit as in standard tests.
- Capacities and instantaneous resistances are estimated accurately.

ARTICLE INFO

Article history:
Received 5 March 2014
Received in revised form
1 July 2014
Accepted 18 July 2014
Available online 28 July 2014

Keywords:
Support vector machine
State-of-health
Capacity
Resistance
Lithium-ion battery
Electric vehicle

ABSTRACT

Capacity and resistance are state-of-health (SOH) indicators that are essential to monitor during the application of batteries on board electric vehicles. For state-of-health determination in laboratory environment, standard battery performance tests are established and well-functioning. Since standard performance tests are not available on-board a vehicle, we are developing a method where those standard tests are applied virtually to a support vector machine-based battery model. This data-driven model is solely based on variables available during ordinary electric vehicle (EV) operation such as battery current, voltage and temperature. This article contributes with a thorough experimental validation of this method, as well as the introduction of new features – capacity estimation and temperature dependence. Typical EV battery usage data is generated and exposed to the suggested method in order to estimate capacity and resistance. These estimations are compared to direct measurements of the SOH indicators with standard tests. The obtained estimations of capacities and instantaneous resistances demonstrate good accuracy over a temperature and state-of-charge range typical for EV operating conditions and allow thus for online detection of battery degradation. The proposed method is also found to be suitable for on-board application in respect of processing power and memory restrictions.

1. Introduction

Electric vehicle (EV) users are particularly impressed by the lack of local air and noise pollution and the low maintenance costs in comparison to conventional combustion-engine-driven cars. However, these users are seriously concerned about EV driving range [1]. Apart from range, the power available for driving the vehicle in different situations, e.g. for acceleration, is important for EV operation. The range of an electric vehicle corresponds mainly to the battery pack's capacity, and the available power relates to the resistance of the battery pack. With time and usage, capacity and resistance experience degradation, which results in another issue with EVs: limited battery lifetime.

An estimation of the battery's capacity and resistance on-board is thus essential in order to rate the battery's performance during operation, i.e. what peak power can be reached or what range to expect. Capacity and resistance estimations provide also a state-of-health (SOH) indication of the battery pack. A reliable SOH estimation not only ensures safe operation, it can also contribute to a smart optimization of battery usage resulting in an eventually extended lifetime.

Battery SOH estimation methods that are described in the scientific literature, however, suffer from one or several shortcomings with respect to on-board application such as battery-specificity, high computational effort, extensive preceding laboratory work (e.g. aging experiments or determination of physical properties),

* Corresponding author. Tel.: +46 8 790 6557.
E-mail address: vklass@kth.se (V. Klass).

http://dx.doi.org/10.1016/j.jpowsour.2014.07.116
0378-7753/

questionable validity for EV operating conditions (e.g. estimations deduced from usage history in laboratory studies) or need for operation interruptions and additional equipment [2–16]. In a recent article [17], we have therefore introduced a novel method that accomplishes battery performance estimation without prior battery knowledge or experimental preparation. We applied an established machine learning method called support vector machines (SVM) to SOH estimation of a battery pack in a plug-in hybrid electric vehicle (PHEV). Without any experimental preparation or need for prior information about the specific battery, data readily available from the battery management system (BMS) collected in PHEV field tests was analyzed with SVM to build a battery model that captured the behavior of the battery at a reasonable computational load. More precisely, the voltage was modeled based on current and state-of-charge (SOC). The battery resistance was then estimated by running a virtual test on the battery model. This virtual test consisted of the current and SOC profiles from a real standard test and yielded a voltage estimation. In that way, the ease of statistical learning modeling from online available signals was combined with the advantage of the general validity of standard performance tests.

Purely data-driven methods for SOH estimation are rather uncommon in literature. There have, however, been several examples where statistical learning methods such as artificial neural networks (ANN) and SVM have successfully been applied for the related SOC estimation [18–21]. Such black box models do not contribute to an improved understanding of the processes in the battery like physical models do. They have though the advantage of being battery-unspecific, as they – in contrast to physical models, empirical models based on aging experiments or models based on equivalent circuits – do not rely on predetermined system parameters or have any connection to physical properties. The aim of such statistical methods is to learn the behavior of the studied system from a large number of examples and find a mathematical system description. ANN suffer from several local minima, whereas SVM find one global solution. SVM, which also can handle nonlinear systems, outperform ordinary regression due to its insensitivity to small changes. Popular application areas for SVM regression are e.g. bioinformatics, financial time series and electricity load forecasting [22–24]. However, a general limitation with data-driven models is that the methods are only valid within the trained data range.

Apart from Ref. [17], we know of one other paper that applied SVM in the context of on-board SOH estimation. That method, however, has a different focus. In Ref. [25], SVM were used to learn the capacity degradation behavior of a battery and to predict remaining useful life (RUL) whereas we use SVM to capture the battery behavior at a point in time by voltage modeling from current and SOC and then estimate SOH indicators via a virtual test of the battery model.

The present study constitutes a continuation of our previous paper [17]. We set here the PHEV field-tested, but non-validated method from that study into a controlled laboratory environment. In contrast to the proof-of-concept character of the previous study, this study aims at increasing understanding of the method's abilities and restrictions with the help of careful investigations enabled by the possibilities of an experimental study. Most decisively, estimation results are to be thoroughly compared to real standard performance tests. Moreover, as it was found in Ref. [17] that temperature is a crucial variable in real-life application, temperature dependence is introduced into the model. Also, the previously presented resistance estimations complemented with capacity estimation, which is an at least equally important SOH indicator for electric vehicle operation, which this study focuses on.

Fig. 1 visualizes the scope of this article. The study compares the SOH figures of merit, capacity and resistance, which are determined in two different ways. The conventional way, which serves as validation, is the derivation of performance values from direct measurements with standard performance tests. Then, the SOH estimation method from Ref. [17] with its two-step procedure of SVM training and virtual tests is applied to battery data generated with a typical EV current profile. In a first step, a SVM is trained with current, temperature and SOC as input and voltage as output. The resulting SVM model serves then as voltage look-up table for hypothetical current/temperature/SOC-input according to the measured current/temperature/SOC-profile from the respective real standard test. The virtual test result can subsequently be used to derive resistance and capacity as in real standard performance tests. The question to be answered is if the capacity and resistance estimations are sufficiently accurate to replace a direct measurement.

2. Methods

2.1. SOH figures of merit

Capacity and resistance are the two properties of a battery cell that are commonly used as measures of battery performance in conventional testing. They capture the most important characteristics of the behavior of the battery and allow therefore for documenting performance degradation with time.

The discharge capacity $Q_{discharge}$ in Ah can be obtained by numerically integrating the current I of a full discharge between specified voltage limits over the discharge time t.

$$Q_{discharge} = \int I dt \tag{1}$$

The internal resistance of a battery cell in Ω can either be measured by electrochemical impedance spectroscopy (EIS) or by a

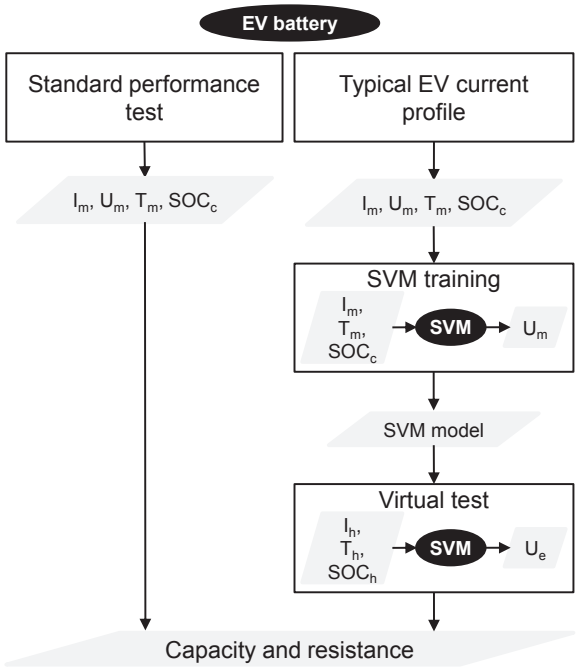

Fig. 1. Schematic overview of the scope of this article. Performance measures of an EV battery cell are determined and compared from real tests as well as from EV battery usage data via support vector machine-based models and virtual tests. I = current, U = voltage, T = temperature, SOC = state-of-charge, m = measured, c = calculated, h = hypothetical, e = estimated.

pulse profile. A common pulse profile for resistance determination is a 10 s maximum current-discharge pulse followed by a 40 s rest period and a 10 s maximum current-charge pulse followed by a 40 s rest period [26,27]. The 10 s discharge resistance R_{10s} is then obtained from the voltage drop $U_{0s} - U_{10s}$ in the voltage response and the applied current I_{max} according to:

$$R_{10s} = \frac{U_{0s} - U_{10s}}{I_{max}}. \quad (2)$$

The 10 s charge resistance can be obtained similarly from the charge pulse.

With time and use, lithium-ion batteries experience performance degradation, commonly called aging. This process can be monitored by tracking the development of capacity and resistance with time. During battery cycling and storage, resistance increases due to a number of processes taking place in the battery such as contact losses in the electrodes and formation of resistive surface films. Capacity on the other hand decreases e.g. as a result from loss of cyclable lithium ions and active electrode material. These so-called aging processes leading to performance degradation vary in extent and type among different cell chemistries and designs and depend on the usage and operating conditions [28].

In combination with some less critical performance measures such as self-discharge and voltage drift, capacity and resistance account for the state-of-health of a battery. The beginning-of-life values are defined to correspond to 100% SOH and the end-of-life of a battery is often regarded to be reached when one of the performance measures has gone below e.g. 80% of the original value.

In the present study, these two most important SOH indicators are determined at one moment in time. The focus is not put on following the SOH of EV batteries with time and usage, although the final on-board application would naturally be to use the SOH indicator estimation for this purpose.

2.2. Experimental procedure

Experiments were performed on commercially available automotive lithium-ion battery cells with specifications [29] as to Table 1. During the experiments, the battery cell under test was placed in a climate chamber (Firlabo, SP-BVEHF) and charged and discharged with a programmable electronic load (Amrel, PLA800-60-300) and a programmable dc power supply (Amrel, SPS8-150-K0E1). Two digital multimeters (Keithley, model 2000 and 2701) delivered the voltage and current measurements with 0.1 s sample intervals (shunt resistor, 0.5 mΩ). For the temperature measurement, a universal analog input module (National Instruments, NI 9219) was used. The temperature was recorded with type K-thermocouples at four positions on the pouch-cell surface: in the center, at the short edge, close to the positive tab at one long edge and close to the negative tab at the opposite long edge. The experimental setup was controlled with a custom-made program in LabVIEW (National Instruments).

The battery cell under test was exposed to an experimental procedure according to Fig. 2. The profile consisted of standard performance tests (Section 2.2.1) as well as a typical EV current profile (Section 2.2.2) at five different climate chamber temperatures from 0 to 40 °C.

Table 1
Specifications of the tested lithium-ion battery cells [29].

Nominal capacity Q_{nom}	17.5 Ah
Maximum voltage U_{max}	4.1 V
Minimum voltage U_{min}	2.5 V
Maximum continuous current I_{max}	35 A
Positive electrode	Mixed oxide
Negative electrode	Hard carbon
Dimensions	253 × 172 × 5.8 mm

2.2.1. Standard performance test

In the standard performance tests (dashed line and dotted line in Fig. 2), a conventional procedure for capacity and resistance tests was performed. The full cycle for the capacity measurement was performed twice and the resistance pulse sequence was performed at four different SOC (90, 70, 50, 30%).

The building blocks of the experimental procedure were:

- acclimatization phase at the respective climate chamber temperature,
- standard charges at C/3 rate to the specified upper voltage limit of 4.1 V with an additional constant voltage step at 4.1 V,
- standard discharges at C/3 rate to the specified lower voltage limit of 2.5 V for capacity determination,
- one-hour rest periods prior to each test,
- partial discharges at C/3 rate in order to reach a certain SOC,
- 10 s charge or discharge pulses at 2C rate followed by 40 s rest periods for resistance determination.

2.2.2. Typical EV current profile

The EV current profile (dash-dotted line in Fig. 2) was based on field test data from the battery pack in a Volvo C30 Electric car. The 24 kWh battery pack in the C30 Electric is composed of 384 single cells of the type from Table 1 that are arranged in 16 modules of 24 cells each with a 12S–2P configuration. An EV duty profile (Fig. 3), which was recorded by Volvo Car Corporation in a Volvo C30 Electric, was chosen. It covers a ΔSOC of about 15% and represents an example of a typical commuting driving cycle. The current profile raw data was interpolated in order to match a time vector with 1 s intervals and scaled down from battery pack to cell level by taking into account the electric configuration of the battery pack. This current profile was applied to a cell at four different SOC regions that match the SOC of the resistance measurements.

2.3. Support vector machine model

The current, voltage and temperature recorded in the EV current profile experiments served as basis for a data-driven battery performance estimation method, which we have presented previously for real-life battery data from field tests [17]. The developed SOH estimation method makes use of support vector machines, a statistical learning method, which can deal with non-linear systems. The general idea is to find a small number of support vectors out of a large number of examples that still describes a system.

The SVM concept as developed by Vapnik [30] is indicated in the following; a more detailed derivation can be found in e.g. Ref. [31]. A SVM training data set consists of L points with input x of dimensionality D and output y.

$$\{x_i, y_i\} \quad \text{where } i = 1, ..., L, y_i \in \Re, x \in \Re^D. \quad (3)$$

The aim is to find a function $f(x)$ that returns the true output y_i with a maximum error of ε for the training data and is as flat as possible. The function for a linear case is shown here with $\langle \cdot, \cdot \rangle$ as scalar product notation:

$$f(x) = \langle w, x \rangle + b. \quad (4)$$

A small w is necessary in order to guarantee the flatness of the function and can be found from minimizing the norm $\|w^2\|$. Slack variables have to be introduced moreover for the case that the optimization problem is not feasible (soft margin). The resulting

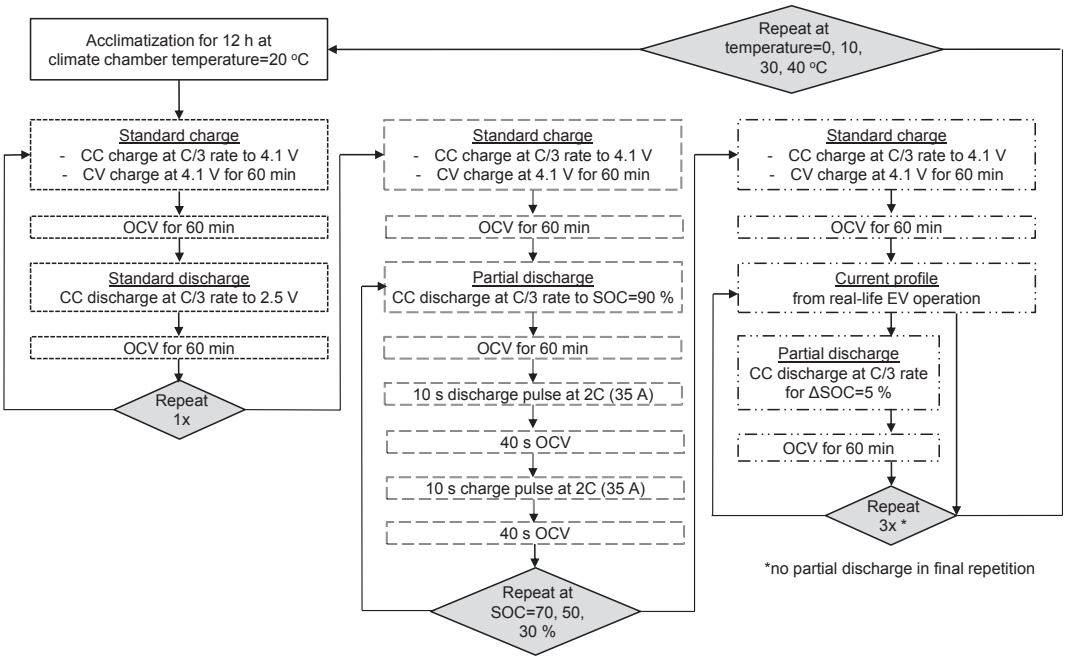

Fig. 2. Detailed description of the three parts of the experimental procedure: standard capacity test (dotted line), standard resistance test (dashed line), typical EV current profile (dash-dotted line). CC = constant current, CV = constant voltage, OCV = open circuit voltage.

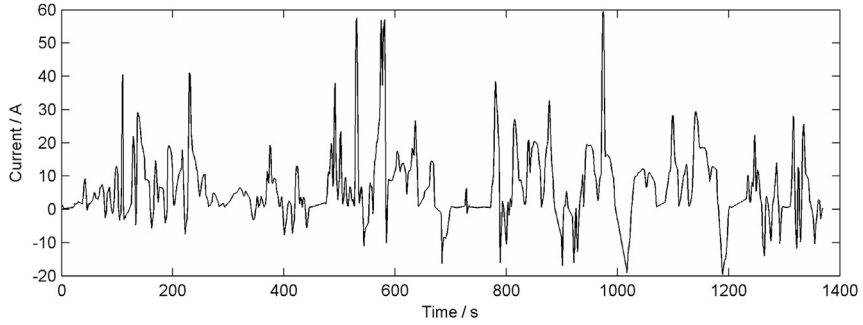

Fig. 3. Current profile downscaled to cell level from an EV duty profile recorded by Volvo Car Corporation in a Volvo C30 Electric.

optimization problem includes a constant C that determines the trade-off between the flatness and the amount up to which errors larger than ε are permitted. Solving of this problem can be simplified by introducing Lagrange multipliers. w can then be computed from a linear combination of the training input and b can be derived from exploiting the Karush–Kuhn–Tucker conditions. The introduction of Lagrange multipliers enables also the extension from linear to non-linear functions. For that purpose, the input data is mapped into a feature space $\Phi(x_i)$ with the help of a kernel function. Here, we apply a radial basis function (RBF) kernel k.

$$k(x_i, x_j) = e^{-\gamma \|x_i - x_j\|^2}, \tag{5}$$

where γ is the kernel option.

In order to estimate battery performance from the raw data, the battery data was subject to SVM training and test as previously illustrated in Fig. 1. The SVM training and test was performed with a SVM implementation in C, SVM^{light} [32], and for the data preparation and analysis MATLAB was used.

For the SVM training, battery models were created from data sets consisting of current, voltage, temperature and either SOC or Ah vectors from the EV current profile experiments. The Ah values were calculated by Coulomb counting (Equation (1)) starting from 0 Ah after the full charge prior to the sequence of current profiles in the experimental procedure. SOC was derived analogously starting from $SOC_{start} = 100\%$ after the full prior charge:

$$SOC\left(t\right) = SOC_{start} - 100 \cdot \frac{\int I dt}{Q}. \tag{6}$$

The capacity value Q for the different temperatures was taken from the average of the two full discharges in the respective test sequence. In the SVM training, current, temperature and either Ah or SOC served as input, whereas voltage was the output variable. An example of a row in a data file for training in SVM^{light} is shown in Table 2. The columns comprise voltage, current, temperature and SOC (or Ah throughput) in the chronological sequence as measured in the laboratory with a time interval of 0.1 s. Detailed information on data preparation (e.g. scaling to [0,1] interval), training procedure and the parameterization and cross-validation can be found in Ref. [17]. In this study, the same SVM parameter set as in Ref. [17] was used: RBF-kernel with $\gamma = 14$, $C = 1.0134$, and $\varepsilon = 0.01$. These values were chosen from a grid search. The training with the SVM^{light}-function svm_learn results into a data file that contains the SVM model.

Table 2
Example of a row in a training data file in SVM^{light}-compatible format. The voltage vector serves as output in the SVM training whereas current, temperature and SOC form the input. The values are scaled to a [0,1] interval.

Voltage	Current	Temperature	SOC
0.833778	1:0.509655	2:0.427182	3:0.747294

2.4. Virtual test

Following the procedure from Fig. 1, the battery model derived in Section 2.3 was tested virtually with a hypothetical input e.g. a capacity or resistance test. For that purpose, the current and either SOC or Ah profiles from real standard tests were applied to the battery model to estimate the voltage response with the SVM^{light}-function svm_classify. This function works as a voltage look-up table from the SVM model data file for the provided current/temperature/SOC (or Ah)-input. The concept has been presented previously in Ref. [17] (see for test procedure, cross-validation etc.) and has been named a virtual test.

The virtual resistance test was performed with a current vector consisting of the aforementioned 10 s discharge and charge pulses in combination with a SOC vector starting from either 90, 70, 50 or 30% SOC. For the capacity estimation, the test input was a constant-current vector at C/3 rate and an Ah vector running from 0 to 14 Ah. The virtual discharge was aligned to real-life battery data that normally contain little or no data at very low SOC. Since SVM naturally perform best within the trained data range, a full battery discharge was avoided. However, the partial capacity still provides a valid SOH indicator. If desired, a temperature vector could be added to the virtual capacity and resistance test inputs.

The virtual tests yielded voltage estimations that served for the derivation of capacity and resistance values according to Equations (1) and (2). The quality of the estimation of capacity and resistance ($X_{estimated}$ where X can be capacity or resistance) for the different operating conditions in comparison to the experimentally measured values $X_{measured}$ was then evaluated with the maximum and minimum relative errors RE in %, the root-mean-square error RMSE in Ah or V and the root-mean-square percentage error RMSPE in %:

$$RE = 100\% \cdot \frac{|X_{estimated} - X_{measured}|}{X_{measured}}, \tag{7}$$

$$RMSE = \sqrt{\frac{1}{n}\sum_{1}^{n}(X_{estimated} - X_{measured})^2}, \tag{8}$$

$$RMSPE = 100\% \cdot \sqrt{\frac{1}{n}\sum_{1}^{n}\left(\frac{X_{estimated} - X_{measured}}{X_{measured}}\right)^2} = \sqrt{\frac{1}{n}\sum_{1}^{n}RE^2} \tag{9}$$

where n is the number of estimations.

3. Results and discussion

This section treats at first exemplary results from experiments (Section 3.1) and SVM modeling (Section 3.2) separately to then turn to a more extensive side-by-side comparison of real and virtual test results including a qualitative evaluation of estimation performance for capacity and resistance (Section 3.3). The results section closes with an overview of the SVM training and test performance in terms of required computational effort (Section 3.4) and a description of an EV implementation scenario of the presented SOH estimation method (Section 3.5).

3.1. Experimental results

Laboratory experiments were performed to obtain SOH indicator measurements (standard performance tests) and to provide battery usage data for SVM training (EV current profile). The measurements from the experimental procedure according to Fig. 2 at 20 °C ambient temperature are exemplarily shown in Fig. 4. The respective results for ambient temperatures of 0, 10, 30 and 40 °C are included in the discussion but not depicted individually.

Fig. 4 illustrates the measurements of voltage, current and temperature with 0.1 s time steps during two capacity tests, a pulse profile at four different SOC and an EV duty profile at the same four SOC. A closer look at Fig. 4(a)–(c) reveals that the intended experimental procedure was not realized at all points in the test. During some charge and discharge pulses, the current is restricted due to the specified voltage limits included in the custom-made control software or the internal limitations of the load. Similar observations can be made for the measurements at 0, 10, 30 and 40 °C.

Rest periods of 60 min are inserted into the experimental procedure to allow the cell to relax before each test. It can be seen in Fig. 4(a) that the OCV still increases marginally after e.g. a one-hour rest phase after a full or partial discharge. Meanwhile, one hour is enough for the temperature to return to the level of ambient temperature after a test as Fig. 4(c) supports. 60 min are consequently not enough to fully relax the cell but it should be a reasonable time period for preventing the prior usage history to impact the test results. These observations apply as well for the measurements at the other four temperature levels.

The temperature measurement in Fig. 4(c) reveals information about the general trend of temperature as well as the temperature distribution in the cell. The temperature increases during the applied profile are moderate. For all four ambient temperatures, the maximum increase from ambient temperature level lies in the range of 1.5–2 °C. The temperature differences between different measurement positions on the cell surface are one magnitude smaller. At 20 °C, the measurement position close to the positive pole shows the highest temperature value out of all measurement positions most of the time (Fig. 4(c)). The temperature is slightly lower at the negative and the temperatures in the center and at the short edge show the lowest value for the largest part of the temperature profile. These temperature distribution observations apply also for the tests at ambient temperature levels of 0 and 10 °C. At 30 and 40 °C, on the other hand, the negative instead of the positive pole stands for the highest temperature for the most part of the temperature profile. Since the variations between temperature measurement positions are small compared to the general trend of temperature, the temperature measurement from the center position, which represents an average temperature on the cell surface, is chosen as temperature input to the SVM training in Section 3.2.

Another observation from the temperature recording in Fig. 4(c) in relation to Fig. 4(a) and (b) is the time shift between processes happening in the cell and the manifestation in a measured temperature decrease or increase. It is a general problem in EV battery pack monitoring that the actual temperature inside a cell is unknown as temperature sensors, which are placed on the surface of the cell, show the temperature development with a time shift and probably also some offset from the real temperature value. However, a method to measure temperature inside a battery cell without negatively affecting the battery performance and safety has to our knowledge not been found yet.

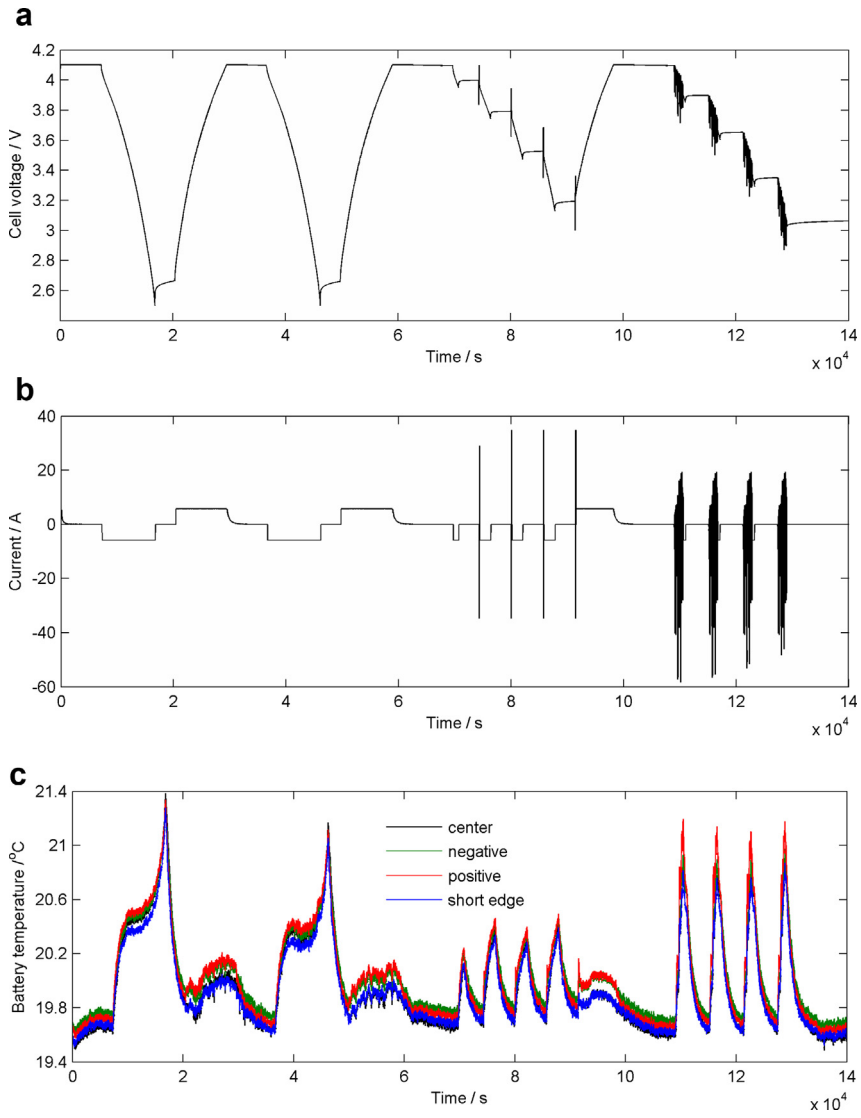

Fig. 4. Measured (a) cell voltage, (b) current and (c) temperature during the experimental procedure according to Fig. 2 at 20 °C. (For colored temperature measurements in Fig. 4(c), please refer to the web version.)

Whereas the battery data collected during the EV current profile experiments served as input to the SVM training in the following section, the capacity and resistance test measurements accounted for the experimental validation of the SOH estimation results. Fig. 5 shows a close-up of a selected capacity and resistance test respectively in order to illustrate the derivation of capacity and resistance by Equations (1) and (2). In Fig. 5(a), the measured voltage response to a 10 s 35 A-discharge pulse of a resistance pulse profile at 90% SOC and 20 °C is shown and Fig. 5(b) displays the voltage measured during two consecutive C/3 rate discharges at 20 °C. Fig. 5 contains also estimated voltage results from the SVM modeling, which will be discussed later in Sections 3.2 and 3.3.

The results from capacity and resistance tests at the examined temperature levels can be found in Figs. 6–8 (solid lines). Generally, it is observed that the instantaneous voltage drop contribution of the resistance (x) is only slightly influenced by different SOC levels for one temperature (Fig. 6). Fig. 7 illustrates that the effect of temperature on the instantaneous voltage drop (x) is more pronounced. Those observations are in accordance with experimental studies on comparable battery chemistry [4]. Fig. 6 shows also the time-dependent drop contribution of the resistance (*). It accounts only for 17% of the total voltage drop for the chosen battery cell and current pulse profile (specified maximum continuous current in 10 s). Fig. 8 summarizes the capacity test results from the two consecutive laboratory tests (first (*) and second (+) discharge) and the average of those tests (x). The difference between the highest and the lowest 4.1–3.0 V capacity at C/3-current for the given temperature interval is as small as about 1 Ah. The capacity increases for increasing temperature as expected.

3.2. SVM models and virtual test results

SVM models are created for data sets from the battery data collected during the EV current profile experiments using the procedure as described in Section 2.3. Four different types of data sets are used:

R. for resistance estimation with a temperature-independent model: voltage, current and SOC data from one single EV current profile at one temperature level,
C. for capacity estimation with a temperature-independent model: voltage, current and Ah data from all four EV current profiles at one temperature level,

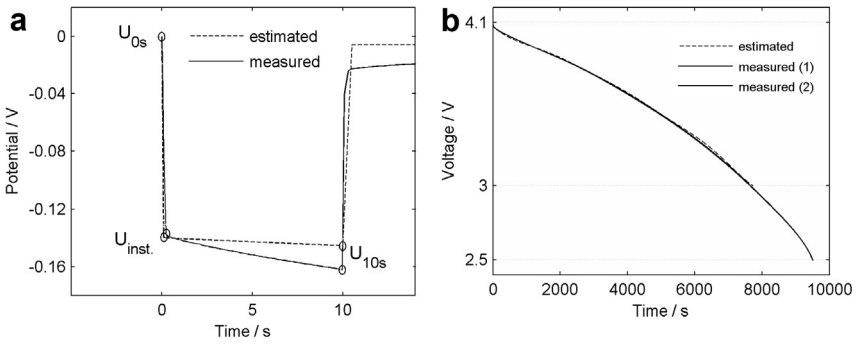

Fig. 5. (a) Estimated (dashed line, temperature-independent model) and measured (solid line) voltage response during a resistance test profile (35 A-discharge pulse for 10 s at 90% SOC and 20 °C). The voltage drop can be separated into an instantaneous drop ($\Delta U_{inst.} = U_{0s} - U_{inst.}$) and a time-dependent drop ($\Delta U_{time\text{-}dep.} = U_{inst.} - U_{10s}$). (b) Estimated (dashed line, temperature-independent model) and measured (solid line) voltage response during capacity test profiles (partial or full discharge at C/3 rate constant current at 20 °C). Two consecutive experimental discharge curves are shown (1 and 2).

RT. for resistance estimation with a temperature-dependent model: voltage, current, SOC and temperature data from all four EV current profiles at all temperature levels,
CT. for capacity estimation with a temperature-dependent model: voltage, current, Ah and temperature data from all four EV current profiles at all temperature levels.

To give an example of SVM training, a case is shown where a SVM is trained with the measured voltage and current and the calculated SOC (Equation (6)) from the EV current profile around the 90% SOC level at 20 °C (type R data). The derived SVM model is then exposed to a virtual resistance test as previously described in Section 2.4. Fig. 5(a) shows the voltage response of this virtual test (dashed line). The estimated voltage curve exhibits a voltage drop as expected during the discharge pulse. In the relaxation period on the other hand, instead of a slow relaxation as anticipated from experiments, the voltage shows the same value under the relaxation period. This behavior results from the fact that the model did not include any dynamics. The 10 s discharge resistance for a 35 A pulse at 90% SOC can be estimated from this virtual voltage response to 4.1 mΩ (Equation (2)). This value as well as the shape of the voltage curve is further discussed in comparison to the corresponding real test in Section 3.3.

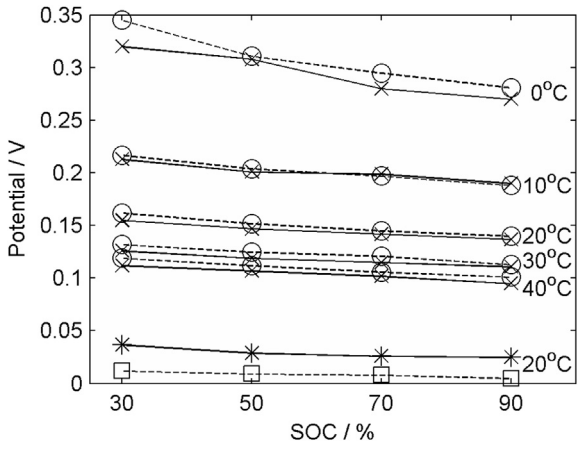

Fig. 6. Measured (solid line) and estimated (dashed line, temperature-independent model) values for the instantaneous voltage drop at 0, 10, 20, 30 and 40 °C and the time-dependent voltage drop at 20 °C vs. SOC. Measured instantaneous drop (x), measured time-dependent drop (*), estimated instantaneous drop (○), estimated time-dependent drop (□).

When capacity instead of resistance is the desired measure of performance to be estimated, a SVM training with voltage, current and Ah data from all EV current profiles at 20 °C as input is performed (type C data). Here, it was decided to use the simple Ah throughput (Equation (1)) instead of SOC to ensure unbiased estimations, as the SOC contains information on the capacity already (Equation (6)). In an online application though, there would be ways to include the capacity in the SVM training input (in the SOC vector) as well as the virtual test output (capacity estimation from the virtual test). The temperature-dependent capacity value needed for the SOC algorithm could then be updated to an up-to-date estimate from the virtual test. Fig. 5(b) shows the virtual test result, i.e. the estimated voltage (dashed line) during a discharge at C/3 rate. The virtual capacity test is designed to cover a partial discharge of 14 Ah as a full discharge is unusual in electric vehicles and SVM perform best within the range of the training data. Instead of the full discharge capacity (4.1–2.5 V), a partial capacity measure has thus been defined. This 4.1–3.0 V capacity can be estimated to 12.45 Ah in Fig. 5(b) (Equation (1)). If the EV driving occasionally provides a full discharge, the total capacity can naturally be estimated. However, for SOH estimation purposes in contrast to SOC estimation, a partial capacity estimate is sufficient.

In real-life applications, where the temperature conditions are not as controlled as in the laboratory, it is important to include temperature in the SVM model. A temperature-independent model would face problems especially with battery performance degradation as the effects of temperature and aging on performance measures have to be distinguished. When the battery experiences aging on-board an electric vehicle, e.g. the resistance increases and the curves in Fig. 7 shift upwards [33]. The model has therefore to be able to include temperature as explaining variable. The data sets of type RT and CT, which cover all five temperature levels, comprise thus temperature data additionally to voltage, current and SOC/Ah. The virtual capacity and resistance tests are also complemented by a temperature vector. It is assumed that the temperature is constant under the virtual tests. The voltage responses of the temperature-dependent virtual resistance and capacity tests are not explicitly shown as they look similar to the temperature-independent results in Fig. 5(a) and (b); the resulting resistance and capacity estimations are, however, presented in Section 3.3.2.

3.3. Comparison of real and virtual tests

This section starts out with an exemplary in-depth comparison of a real/virtual test pair for resistance and capacity estimation respectively. The second subsection covers then all resistance and

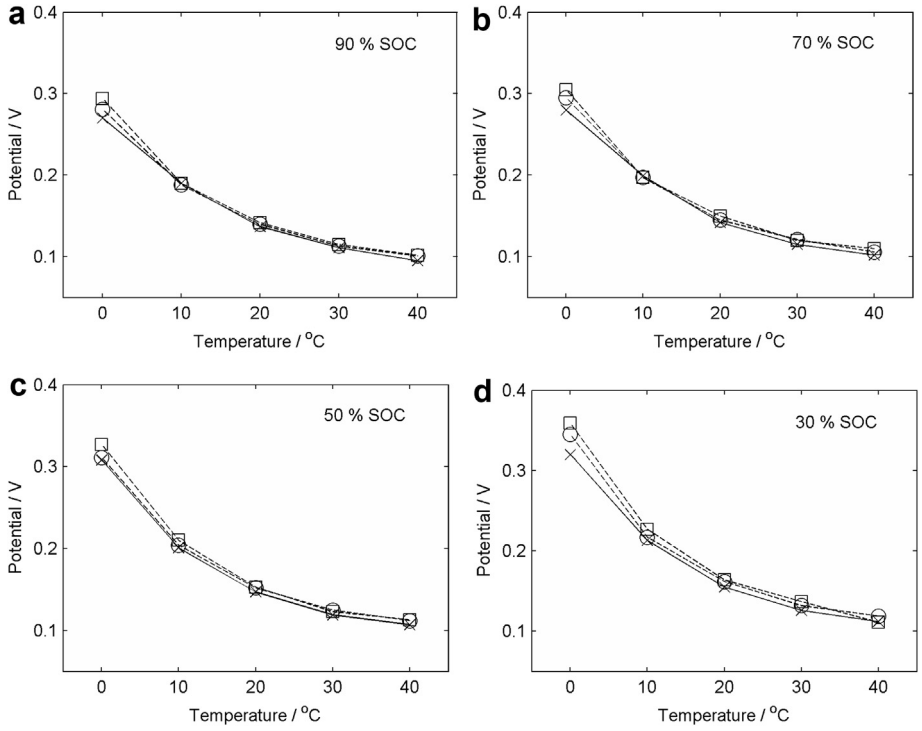

Fig. 7. Instantaneous voltage drop at (a) 90%, (b) 70%, (c) 50% and (d) 30% SOC for 0, 10, 20, 30 and 40 °C. Measured (x, solid line) and estimated values (dashed line) from a temperature-independent (○) or temperature-dependent (▫) SVM model.

capacity measurement and estimation results from the temperature-independent and the temperature-dependent model.

3.3.1. *Example of a real/virtual test comparison*

Fig. 5 shows real resistance and capacity tests together with the respective virtual tests based on data sets of type R and C respectively. The 10 s discharge resistances, which can be derived from Fig. 5(a), are 4.6 mΩ for the laboratory test and an estimation of 4.1 mΩ for the virtual test based on the temperature-independent model (Equation (2)). A closer look at the voltage responses provides information about the origins of the resistance estimation error of 11%. Generally, a discharge current pulse resistance can be divided into two contributions: Instantaneously when the current is applied, a voltage drop $\Delta U_{\text{inst.}}$ occurs that can be related to ohmic losses, contact resistance and activation overpotential [2]. The time-dependent further drop $\Delta U_{\text{time-dep.}}$, which increases during the pulse time, is connected to the SOC decrease and the diffusion in the electrolyte and the active materials ($\Delta U_{\text{time-dep.}} = \Delta U_{\text{SOC}} + \Delta U_{\text{diffusion}}$). These voltage drop regions are indicated in Fig. 5(a). The instantaneous voltage drop ($\Delta U_{\text{inst.}} = U_{0s} - U_{\text{inst.}}$) is estimated accurately (140 mV estimated vs. 137 mV measured). The estimation of the time-dependent drop ($\Delta U_{\text{time-dep.}} = U_{\text{inst.}} - U_{10s}$) deviates, however, considerably (5 mV estimated vs. 25 mV measured). The small estimated decrease in voltage can be related to the SOC decrease during the pulse as current integration illustrates: The charge that leaves the battery during the 10 s 35 A CC discharge pulse corresponds to a $\Delta U = 0.006$ V in Fig. 5(b) (measured); a voltage drop that matches well the estimation of $\Delta U_{\text{time-dep.}} = 0.005$ V from the virtual test. The good agreement of ΔU_{SOC} and the estimated $\Delta U_{\text{time-dep}}$ applies for all temperature and SOC levels included in this study. Therefore, it can be concluded that the estimated value of $\Delta U_{\text{time-dep.}}$ actually only includes the voltage drop due to the SOC decrease ΔU_{SOC}. A part of the resistance estimation error as well as the lack of proper relaxation (Section 3.2) can thus be explained with the static model formulation. A $\Delta U_{\text{time-dep.}}$-estimation including $\Delta U_{\text{diffusion}}$ can simply not be expected. It seems therefore practical for the model evaluation to look at the two contributions of the total discharge resistance separately. The separation into the instantaneous and the time-dependent contribution will be applied in the rest of the paper.

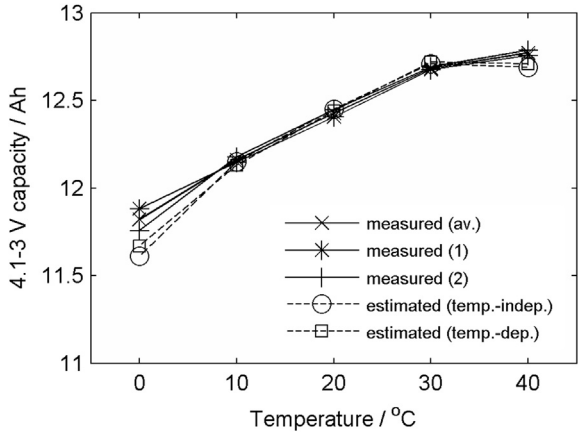

Fig. 8. Measured (solid line) and estimated (dashed line) 4.1–3.0 V-capacity for 0, 10, 20, 30 and 40 °C. Estimated capacity based on temperature-independent (○) and temperature-dependent (▫) model, measured capacity of the first (*) and second (+) discharge, average value of the capacities of the first and second discharge (x).

A virtual capacity test result is depicted together with real capacity tests in Fig. 5(b). The estimated voltage (dashed line) predicts the experimentally determined discharge curves very accurately (solid lines). For the example of 20 °C as illustrated here, the estimated partial capacity of 12.45 Ah (Equation (1)) matches the measured partial capacities of 12.41 and 12.45 Ah (first and second discharge in Fig. 5(b)) with an estimation error of 0.32 and 0% respectively. As mentioned earlier in Section 3.2, the virtual test

was designed to evaluate the 4.1–3.0 V capacity due to restricted availability of real-life data at low SOC. The 4.1–3.0 V capacity still provides a valid SOH indication and at this temperature and rate it corresponded to about 80% of the total measured capacity between 4.1 and 2.5 V.

3.3.2. Estimation performance

The discharge resistances at 90, 70, 50 and 30% SOC are estimated from SVM models based on the EV current profile data sets of type R and RT (Section 3.2) at 0, 10, 20, 30 and 40 °C.

Fig. 6 summarizes the results for the two parts of the discharge resistance from the temperature-independent model. The virtual test greatly underestimates the measured value of the time-dependent drop (*) as can be seen for the example of the 20 °C data. The RMSE and RMSPE for all temperatures read 29 mV and 74% (Table 3). This underestimation originates from the disregarded diffusion drop as discussed before (Section 3.3.1). The time-dependent voltage drop estimations will therefore not be considered further in the following. The SVM estimation of the instantaneous voltage drop (o) on the other hand slightly overestimates the measured laboratory value (x) in most cases (Figs. 6 and 7). Still, the estimation with the temperature-independent model is satisfactorily accurate with a RMSE of 8.2 mV and a RMSPE of 4.2% for the 20 estimations at different operating conditions (Table 3). The estimation error is larger than average for low temperatures and low SOC (maximum relative error = 7.8%) and the best estimation is achieved at moderate temperatures and high to medium SOC (minimum relative error = 0.97%).

Fig. 7, which plots the instantaneous resistance contribution versus temperature instead of SOC, shows additionally the results from the temperature-dependent SVM model (□). The overall estimation from the temperature-dependent model (□, RMSPE = 6.2%) is slightly inferior to the temperature-independent one (o, RMSPE = 4.2%). From Fig. 7, it can be observed that the inferiority mainly originates from the estimation at 0 °C. The two estimations from the temperature-dependent and temperature-independent model are close for the other temperatures. This applies for all studied SOC levels (Fig. 7(a)–(d)).

The 4.1–3.0 V-capacity estimations based on the temperature-dependent (type CT data) and the temperature-independent (type C data) models are illustrated in comparison to the results from the real capacity tests in Fig. 8. The estimations based on the temperature-independent (o) and the temperature-dependent model (□) lie very close to the actual values for 10–30 °C. The estimations for 0 and 40 °C deviate somewhat more while the experimental values at 0 °C actually also show a significant variation. The RMSPE of the temperature-independent model for all temperatures is 0.85%, rendering an accurate capacity estimation (Table 3). The estimations based on the temperature-dependent model are even slightly closer to the laboratory results (x,*,+) with a RMSPE of 0.63%. More estimation performance figures can be found in Table 3.

3.4. Computational performance

In practice, the performance of a SVM model consists of both the estimation performance (Section 3.3.2) and the computational performance. This section deals with the latter with respect to the memory and processing power that are needed in order to achieve the previously presented results. SVM training and SVM test require a certain runtime that is given in core-s and the SVM model resulting from the SVM training is made up of a certain number of support vectors (SV). Generally, less complex models with a low number of SV and fast training times are preferable whereas the time and space requirements normally grow with the size of the problem, i.e. the number of training variables and examples. Besides estimation accuracy, the number of support vectors and the training time can also serve as selection criteria for SVM model parameters such as kernel choice (see Section 2.3), which are fixed here, or for the selection of appropriate variables [34]. All SVM trainings and tests are performed on an AMD Athlon II X2 B24 processor with 3 GHz frequency.

Table 4 summarizes the computational performance of all SVM trainings and SVM models of this study. For SVM models from type R data sets, the number of support vectors is observed to increase with falling temperature and lower SOC, i.e. the maximum number of SV of 1760 is reached for 30% SOC at 0 °C and the minimum number of SV of 29 is derived for 90% SOC at 30 °C (40 °C value lies close at 33 SV). The training runtime behaves accordingly with the highest value of 35 core-s and the lowest value of 0.60 core-s. The testing runtime is fast, lying under 30 core-ms for all virtual resistance tests based on type R data.

For type C data, the number of support vectors and the training runtime are lowest for the data set at 40 °C with 299 SV and a training runtime of about $6.0 \cdot 10^2$ core-s. The values increase up to a number of 13,127 SV and a training runtime of about $2.8 \cdot 10^4$ core-s for the case of the 0 °C data set. The test runtime stretches from 32 to 0.4 core-s.

The SVM training for data of type RT results in 10,635 support vectors. The large number of examples in the data set covering the whole SOC-operating range at different temperatures (880,233 examples) results in a long training runtime of $2.1 \cdot 10^5$ core-s. In comparison to the SVM models based on type R data, the training with type RT data yields about twice as many support vectors as the sum of all support vectors of all type R models of 4769 SV (Table 4). Also the training runtime exceeds the sum of type R runtimes of 105 core-s by a factor of about 2000. The 20 virtual resistance tests, which are performed on this temperature-dependent SVM model, take about 0.2 core-s each.

The data set of type CT is chosen in order to estimate capacity with the help of a temperature-dependent model. The training takes $1.6 \cdot 10^5$ core-s. It exceeds the sum of the training runtimes of all data sets of type C of $4.4 \cdot 10^4$ core-s by a factor of about 4 (Table 4). The number of support vectors of 9670 for the SVM model from data set CT on the other hand is about a factor of 2 lower than the sum of the support vectors from the individual models from data sets C of 22,087 SV. The smaller number of SV indicates that temperature is an explaining variable that decreases the complexity of the SVM model. The virtual capacity test runtimes at the five temperature levels span from 17 to 19 core-s.

As a result from the strongly increased number of support vectors and training runtime for type RT in comparison to type R data, an additional special case is examined. A SVM training is

Table 3
Summary of the estimation performance of the temperature-independent and the temperature-dependent model for the 4.1–3.0 V-capacity and the instantaneous potential drop. RMSE = root-mean square error, RMSPE = root-mean square percentage error, RE = relative error (Equations (7)–(9)).

SVM model type	Estimation quantity	Number of elements	RMSE/mV or Ah	RMSPE/%	Max. RE/%	Min. RE/%
Temperature-independent	Instantaneous potential drop	20	8.2 mV	4.2	7.8	0.97
	4.1–3.0 V-capacity	5	0.10 Ah	0.85	1.8	0.10
Temperature-dependent	Instantaneous potential drop	20	14 mV	6.2	12	0
	4.1–3.0 V-capacity	5	0.076 Ah	0.63	1.3	0.11

Table 4
Overview of the computational SVM performance for the studied data sets. The training data sets are specified by the data type (R, C, RT, CT, see Section 3.2), the SOC level of the current profile (CP90-30), the temperature level (0–40 °C) and the number of examples. Training performance is evaluated in respect of number of support vectors and approximate training runtime in core-s. The virtual tests, which have been performed on the resulting SVM models, are indicated.

Training data set				Number of SV	Runtime/core-s	Performed virtual tests
Type	CP	Temperature/°C	Number of examples			
R	90	0	12,461	289	6.2	Resistance at 90% SOC and 0 °C
R	70	0	12,271	448	10	Resistance at 70% SOC and 0 °C
R	50	0	12,656	750	18	Resistance at 50% SOC and 0 °C
R	30	0	12,099	1760	35	Resistance at 30% SOC and 0 °C
R	90	10	12,474	78	2.0	Resistance at 90% SOC and 10 °C
R	70	10	12,620	94	2.3	Resistance at 70% SOC and 10 °C
R	50	10	12,706	145	3.6	Resistance at 50% SOC and 10 °C
R	30	10	12,893	521	12	Resistance at 30% SOC and 10 °C
R	90	20	12,555	41	1.1	Resistance at 90% SOC and 20 °C
R	70	20	12,471	66	1.3	Resistance at 70% SOC and 20 °C
R	50	20	12,591	63	1.5	Resistance at 50% SOC and 20 °C
R	30	20	12,601	126	3.2	Resistance at 30% SOC and 20 °C
R	90	30	12,492	29	0.67	Resistance at 90% SOC and 30 °C
R	70	30	12,550	56	1.2	Resistance at 70% SOC and 30 °C
R	50	30	12,517	58	1.3	Resistance at 50% SOC and 30 °C
R	30	30	12,543	69	1.5	Resistance at 30% SOC and 30 °C
R	90	40	12,242	33	0.60	Resistance at 90% SOC and 40 °C
R	70	40	12,337	37	0.68	Resistance at 70% SOC and 40 °C
R	50	40	12,481	45	0.97	Resistance at 50% SOC and 40 °C
R	30	40	12,245	61	1.1	Resistance at 30% SOC and 40 °C
C	90–30	0	178,901	13127	$2.8 \cdot 10^4$	Capacity at 0 °C
C	90–30	10	188,801	5647	$1.1 \cdot 10^4$	Capacity at 10 °C
C	90–30	20	178,201	2135	$3.9 \cdot 10^3$	Capacity at 20 °C
C	90–30	30	170,201	879	$1.7 \cdot 10^3$	Capacity at 30 °C
C	90–30	40	164,129	299	$6.0 \cdot 10^2$	Capacity at 40 °C
RT	90	0–40	121,905	483	$3.6 \cdot 10^2$	Resistance at 90% SOC and 0, 10, 20, 30, 40 °C
RT	90–30	0–40	880,233	10635	$2.1 \cdot 10^5$	Resistance at 90, 70, 50, 30% SOC and 0, 10, 20, 30, 40 °C
CT	90–30	0–40	880,233	9670	$1.6 \cdot 10^5$	Capacity at 0, 10, 20, 30, 40 °C

performed with only the first current profile (CP90) from the RT data set instead of all current profiles (CP90-30). The SVM model derived in this way has 483 SV and takes 360 core-s to train. This result compares to the sum of all SV of 470 and the sum of all training runtimes of 11 core-s for type R data of CP90 at all temperatures (Table 4). The number of SV is comparable in contrast to the full SOC range data set RT CP90-30 that showed a much higher number of SV than all R data sets. This indicates that a division of the input data in e.g. SOC classes could be reasonable. It can be shown that the division of the input data into SOC classes does not influence the estimation performance negatively. A similar strategy can be applied to type CT data. In order to estimate the 4.1–3.0 V capacity, only a SVM model of the SOC region around 3.0 V is needed. In this way, the training runtime could be decreased considerably.

To conclude about the presented SVM trainings, the number of support vectors that is needed for the evaluated SVM battery models stays reasonably small even for expansive data sets. Those amounts of support vectors should thus be manageable within on-board memory restrictions. The number of support vectors is comparable to a study where SVM were applied to SOC estimation and a comparable amount of input data to data sets of type RT and CT is used ($16 \cdot 10^4$ s simple CC charge–discharge cycle profile) [35]. Anton et al. derived 12,984 SV for SOC estimation from current, voltage and temperature.

The training runtime, however, is improvable. The slow SVM training for expansive data sets of type RT and CT raises questions about the on-board suitability of SVM training. In practice, the training data could be reduced depending on the available online processing power. This could either be achieved by an appropriate preparation, e.g. by a reduction of the amount of data points or a separation of the training data in different groups of temperature and SOC as the shorter training runtimes for data sets R, C and the special case of data type RT restricted to CP90 indicate. In some cases, offline training might be an attractive option, for example when SOH estimates are only desired at regular maintenance occasions. Finally, it can be also considered that processing power and memory capabilities rapidly evolve promising a smooth future application of this kind of methods.

The SOH estimation itself, e.g. the virtual test runtime, is found to be fast for all types of underlying SVM models and is thus suitable for on-board SOH estimation.

3.5. Vehicle implementation scenario

In this section, an implementation scenario of the presented SOH estimation method in an electric vehicle is described in order to illustrate the practical application potential of the method.

Whenever the SOH of an EV battery pack integrated into a vehicle is of interest, the presented method could be used. In order to get an up-to-date SOH indicator estimation, the vehicle has to be driven some amount of time, e.g. 15 min. During that time, relevant data (current, voltage, SOC, temperature) would be collected and stored in the on-board memory. After the specified time, the SVM training would be performed, resulting in a SVM battery model covering the data range of the collected data. In a next step, virtual resistance and capacity tests corresponding to standard performance tests would be initiated. The virtual tests would have to lie within the SVM model data range. Apart from the previously mentioned SOC matching (partial capacity), a matching of the virtual test current and temperature to the SVM model data range would have to be performed in order to consider a variety of duty profiles and different operating temperatures throughout the year. In practice, climate systems of today's commercial EVs ensure, however, a rather narrow operating temperature window for the battery pack. The resistance and capacity estimation results from

those virtual tests could then be set into relation to beginning-of-life battery properties and/or previously derived online SVM-based SOH estimation results at the same conditions (temperature, SOC, current). In that way, the EV user would be able to follow the battery pack's degradation and even more decisive, the car manufacturers could include the SOH information into the BMS in order to ensure safe operation and improve battery usage.

4. Conclusions

A SOH estimation method based on SVM models and virtual standard performance tests has been validated, developed further and evaluated. It requires neither preceding laboratory work, nor operation interruptions and additional equipment.

SVM are found to be a powerful method for handling large amounts of battery data. Battery models can conveniently be created from sets of current, voltage, SOC/Ah and temperature data. In real-life applications where a large range of operating temperatures can be anticipated, a temperature-dependent model is necessary. The temperature-independent model, however, gives equally good estimations in a constant temperature environment. It might be beneficial to split up the data sets in SOC or temperature level classes in order to achieve training time reductions in certain cases. The number of support vectors for the derived SVM models is manageable and should allow the storage in on-board memory. The virtual tests for battery SOH estimation show fast testing times suitable for online usage.

The validation of the SOH estimation method is based on battery data from experimental work. The experiments cover standard performance tests and EV current profiles that serve as input data to the SVM modeling. The estimated SOH indicators show good agreement with the experimentally measured results. The temperature-dependent model specifically estimates the instantaneous voltage drop for 90–30% SOC with a RMSE of 14 mV and the 4.1–3.0 V capacity with 0.076 Ah RMSE for 0–40 °C temperature range. The estimations are thus found to be suitable for on-board detection of battery degradation. Some trade-offs from conventional standard performance testing have however to be made in the virtual tests: The resistance estimation is cut down to the instantaneous part as a result of a lack of dynamics in the model, and a partial capacity is estimated with respect to common SOC ranges during EV operation. The presented model already gives accurate estimations, but for further improvements, dynamics should be added – especially for driving cycles where the diffusion contribution of the resistance is of larger importance than in the studied system.

When aiming for an optimum SOH estimation out of the on-board available information without additional equipment, need for maintenance or preceding laboratory work, a compromise between a simple, computation-modest method and the accuracy of the estimation has to be made. Our contribution is a method for estimating SOH indicators from real-life battery data in a way that increases the comparability between experiments and modeling, i.e. real and virtual tests.

Acknowledgments

This work is supported by the Swedish Hybrid Vehicle Centre (SHC). We thank Anders Bern at Volvo Car Corporation for kindly providing us with field test data as well as the battery cells for laboratory testing. Thanks also to Pontus Svens and Scania for lending us equipment.

References

[1] M. Wikström, Delårsrapport Av Elbilsupphandlingen Januari – Juni 2012, 2012.
[2] A. Nyman, T.G. Zavalis, R. Elger, M. Behm, G. Lindbergh, J. Electrochem. Soc. 157 (2010) A1236.
[3] M. Doyle, T.F. Fuller, J. Newman, J. Electrochem. Soc. 140 (1993) 1526.
[4] J. Belt, V. Utgikar, I. Bloom, J. Power Sources 196 (2011) 10213.
[5] M. Safari, M. Morcrette, A. Teyssot, C. Delacourt, J. Electrochem. Soc. 157 (2010) A892.
[6] K.L. Gering, S.V. Sazhin, D.K. Jamison, C.J. Michelbacher, B.Y. Liaw, M. Dubarry, M. Cugnet, J. Power Sources 196 (2011) 3395.
[7] M. Dubarry, B.Y. Liaw, J. Power Sources 174 (2007) 856.
[8] A. Eddahech, O. Briat, N. Bertrand, J.-Y. Delétage, J.-M. Vinassa, Int. J. Electr. Power 42 (2012) 487.
[9] U. Tröltzsch, O. Kanoun, H.-R. Tränkler, Electrochim. Acta 51 (2006) 1664.
[10] G.L. Plett, J. Power Sources 134 (2004) 252.
[11] G.L. Plett, J. Power Sources 134 (2004) 262.
[12] G.L. Plett, J. Power Sources 134 (2004) 277.
[13] D. Andre, C. Appel, T. Soczka-Guth, D.U. Sauer, J. Power Sources 224 (2013) 20.
[14] D. Andre, A. Nuhic, T. Soczka-Guth, D.U. Sauer, Eng. Appl. Artif. Intel. 26 (2013) 951.
[15] Z. Chen, C.C. Mi, Y. Fu, J. Xu, X. Gong, J. Power Sources 240 (2013) 184.
[16] Y.-H. Chiang, W.-Y. Sean, J.-C. Ke, J. Power Sources 196 (2011) 3921.
[17] V. Klass, M. Behm, G. Lindbergh, J. Electrochem. Soc. 159 (2012) A1856.
[18] T. Hansen, C.-J. Wang, J. Power Sources 141 (2005) 351.
[19] J.C. Álvarez Antón, P.J. García Nieto, C. Blanco Viejo, J.A. Vilán Vilán, IEEE Trans. Power Electron. 28 (2013) 5919.
[20] X. Wu, L. Mi, W. Tan, J.L. Qin, M.N. Zhao, Adv. Mater. Res. 211-212 (2011) 1204.
[21] W. Junping, C. Quanshi, C. Binggang, Energy Convers. Manag. 47 (2006) 858.
[22] H.-X. Zhou, S. Qin, Bioinformatics 23 (2007) 2203.
[23] F.E.H. Tay, L. Cao, Omega 29 (2001) 309.
[24] P. Pai, W. Hong, Electr. Power Syst. Res. 74 (2005) 417.
[25] A. Nuhic, T. Terzimehic, T. Soczka-Guth, M. Buchholz, K. Dietmayer, J. Power Sources 239 (2013) 680.
[26] INL/EXT-07–12536, Battery Test Manual for Plug-in Hybrid Electric Vehicles, 2008.
[27] ISO 12405–1, Electrically Propelled Road Vehicles – Test Specifications for Lithium-ion Traction Battery Packs and Systems – Part 1: High-power Applications, 2011.
[28] T.G. Zavalis, M. Klett, M.H. Kjell, M. Behm, R.W. Lindström, G. Lindbergh, Electrochim. Acta 110 (2013) 335.
[29] www.enerdel.com, April 16, 2013.
[30] C. Cortes, V. Vapnik, Mach. Learn. 20 (1995) 273.
[31] A.J. Smola, B. Schöllkopf, Stat. Comput. 14 (2004) 199.
[32] T. Joachims, Making Large-scale SVM Learning Practical, in: Advances in Kernel Methods Support Vector Learning, MIT-Press, 1999.
[33] S. Käbitz, J.B. Gerschler, M. Ecker, Y. Yurdagel, B. Emmermacher, D. André, T. Mitsch, D.U. Sauer, J. Power Sources 239 (2013) 572.
[34] M.H. Nguyen, F. de la Torre, Pattern Recognit. 43 (2010) 584.
[35] J.C. Álvarez Antón, P.J. García Nieto, F.J. de Cos Juez, F. Sánchez Lasheras, M. González Vega, M.N. Roqueñí Gutiérrez, Appl. Math. Model. 37 (2013) 6244.